

A novel method for estimating shortwave direct radiative effect of above-cloud aerosols using CALIOP and MODIS data

Zhibo Zhang^{*1,2}, Kerry Meyer^{3,4}, Steven Platnick⁴, Lazaros Oreopoulos⁴, Dongmin Lee^{4,5} and Hongbin Yu^{4,6}

1. Department of Physics, University of Maryland, Baltimore County (UMBC), Baltimore, MD, USA
 2. Joint Center Earth Systems & Technology (JCET), UMBC, Baltimore, MD, USA
 3. Goddard Earth Sciences Technology and Research (GESTAR), Universities Space Research Association, Columbia, MD, USA
 4. NASA Goddard Space Flight Center, Greenbelt, Maryland, USA
 5. Goddard Earth Sciences Technology and Research (GESTAR), Morgan State University, Baltimore, MD, USA
 6. Earth System Science Interdisciplinary Center, University of Maryland, College Park, MD, USA
- Corresponding author at: Department of Physics, UMBC, Baltimore, MD, 21250, USA, Tel: 410-455-6315,
Email: Zhibo.Zhang@umbc.edu (Z. Zhang)

Revised for AMT

1 **Abstract**

2 This paper describes an efficient and unique method for computing the shortwave
3 direct radiative effect (DRE) of aerosol residing above low-level liquid-phase clouds
4 using CALIOP and MODIS data. It addresses the overlap of aerosol and cloud rigorously
5 by utilizing the joint histogram of cloud optical depth and cloud top pressure while also
6 accounting for subgrid-scale variations of aerosols. The method is computationally
7 efficient because of its use of grid-level cloud and aerosol statistics, instead of pixel-level
8 products, and a pre-computed look-up table based on radiative transfer calculations. We
9 verify that for smoke over the southeast Atlantic Ocean the method yields a seasonal
10 mean *instantaneous* (approximately 1:30PM local time) shortwave DRE of above cloud
11 aerosol (ACA) that generally agrees with more rigorous pixel-level computation within
12 4%. We also estimate the impact of potential CALIOP aerosol optical depth (AOD)
13 retrieval bias of ACA on DRE. We find that the regional and seasonal mean
14 *instantaneous* DRE of ACA over southeast Atlantic Ocean would increase, from the
15 original value of 6.4 W m^{-2} based on operational CALIOP AOD to 9.6 W m^{-2} if CALIOP
16 AOD retrieval are biased low by a factor of 1.5 (Meyer et al., 2013) and further to 30.9 W
17 m^{-2} if CALIOP AOD retrieval are biased low by a factor of 5 as suggested in (Jethva et
18 al., 2014). In contrast, the instantaneous ACA radiative forcing efficiency (RFE) remains
19 relatively invariant in all cases at about $53 \text{ W m}^{-2} \text{ AOD}^{-1}$, suggesting a near linear relation
20 between the instantaneous RFE and AOD. We also compute the annual mean
21 instantaneous shortwave DRE of light-absorbing aerosols (i.e., smoke and polluted dust)
22 over global oceans based on 4 years of CALIOP and MODIS data. We find that the
23 variability of the annual mean shortwave DRE of above-cloud light-absorbing aerosol is
24 mainly driven by the optical depth of the underlying clouds. While we demonstrate our

- 1 method using CALIOP and MODIS data, it can also be extended to other satellite data
- 2 sets, as well as climate model outputs.
- 3

1

2 **1. Introduction**

3 The shortwave direct radiative effect (DRE) of aerosols at the top of the atmosphere
4 (TOA) is strongly dependent on the reflectance of the underlying surface. Over dark
5 surfaces (e.g. ocean, vegetated land), the scattering effect of aerosols is generally
6 dominant, leading to negative DRE (i.e., cooling) at TOA (Yu et al., 2006). In contrast,
7 when light-absorbing aerosols occur above clouds or other bright surfaces (such as snow,
8 ice, desert), aerosol absorption is significantly amplified by cloud or surface reflection,
9 offsetting or even exceeding the scattering effect of the aerosol, leading to a less negative
10 or even positive (i.e., warming) TOA DRE (Abel et al., 2005; Keil and Haywood, 2003;
11 Twomey, 1977). Therefore, in order to understand the full complexity of aerosol radiative
12 effects on climate, it is important to quantify the DRE under both clear-sky and cloudy-
13 sky conditions. Although the DRE of aerosols in clear-sky regions has been extensively
14 studied and is relatively well constrained based on advanced satellite remote sensing
15 measurements acquired in the last decade (Yu et al., 2006), the cloudy-sky DRE is
16 generally assumed to be negligible or simulated by models (Schulz et al., 2006).
17 Currently model simulations shows a large inter-model spread in cloudy-sky DRE
18 (Schulz et al., 2006), which results from inter-model differences in both aerosol and
19 cloud properties (Schulz et al., 2006; Stier et al., 2013). Therefore, there is a clear need
20 for an observational constraint on the DRE of above-cloud aerosol (ACA).

21 Recent advances in satellite remote sensing techniques have provided an
22 unprecedented opportunity for studying the DRE of ACA. In particular, the availability of
23 measurements from the space-borne Cloud-Aerosol Lidar with Orthogonal Polarization

1 (CALIOP) sensor onboard NASA's Cloud-Aerosol Lidar and Infrared Pathfinder
2 Satellite Observations (CALIPSO) satellite has provided a revolutionary global view of
3 the vertical distribution of aerosols and clouds (e.g., Winker et al., 2013). Using CALIOP
4 aerosol and cloud layer products, Devasthale and Thomas (2011) found frequent
5 occurrences of aerosols residing above low-level clouds in several regions of the globe.
6 In particular, they found a high frequency of smoke occurrence over low clouds in the
7 southeast Atlantic, western coasts of South America (e.g., Columbia, Ecuador, and Peru)
8 and southern Asia. These authors also found a high frequency of natural and polluted dust
9 aerosols overlapping low clouds off the western coasts of Saharan Africa in boreal
10 summer and over boundary layer clouds in the eastern coast of China in boreal spring
11 (see Fig. 3 of Devasthale and Thomas, 2011).

12 CALIOP measurements of ACA properties, in combination with satellite cloud
13 products from, for example, the Moderate Resolution Imaging Spectroradiometer
14 (MODIS), have been used in several recent studies to derive the DRE of ACA with
15 radiative transfer simulations (e.g., Chand et al., 2009; Costantino and Bréon, 2013b;
16 Meyer et al., 2013; Oikawa et al., 2013). (Chand et al., 2009) used CALIOP above-cloud
17 AOD retrievals (Chand et al., 2008) and Terra-MODIS cloud products, both aggregated
18 to 5° gridded monthly means, to calculate the radiative effects of smoke transported
19 above the low-level stratocumulus deck in the southeastern Atlantic. A major point made
20 in this study was that the all-sky DRE of elevated light-absorbing aerosols, such as
21 transported smoke, is strongly modulated by the underlying cloud properties. However,
22 the spatial-temporal aggregation of both CALIOP and MODIS data to coarse gridded
23 monthly means obscures the potential influence of cloud and aerosol variability on the

1 DRE. In particular, using grid box mean cloud optical depth for DRE calculation might
2 lead to biases in DRE due to the plane-parallel albedo bias (Oreopoulos et al., 2007).
3 Moreover, the MODIS level-3 aggregation algorithm samples all liquid water clouds,
4 regardless of possible retrieval contamination by ACA. As a result, the total population of
5 liquid water clouds in the MODIS level-3 products (daily or monthly) may be
6 significantly different from that of below-aerosol-only cloud population. Therefore, using
7 level-3 MODIS products without distinguishing below-aerosol-only from total cloud
8 population can potentially lead to significant errors. The problem could be further
9 complicated by biases in MODIS cloud retrievals associated with the presence of
10 overlying light-absorbing aerosols. When a cloud-pixel is contaminated by overlying
11 light-absorbing aerosols the MODIS cloud optical depth (COD) retrieval is generally
12 biased low (e.g., Coddington et al., 2010; Haywood et al., 2004; Jethva et al., 2013;
13 Wilcox, 2010), an effect not considered in most previous studies (e.g., Chand et al., 2009;
14 Costantino and Bréon, 2013b; Oikawa et al., 2013). Most recently however, (Meyer et al.,
15 2013) collocated CALIOP above-cloud AOD and Aqua-MODIS cloud properties at the
16 pixel level, and the DRE was then computed at these individual collocated pixels. They
17 found that correcting the MODIS COD bias due to ACA contamination can lead to a
18 more positive ACA DRE. Such rigorous collocation has obvious advantages as it takes
19 into account the sub-grid variability of clouds and aerosols, but is on the other hand
20 computationally expensive since it requires large amounts of pixel-level data that make
21 global scale and multiyear studies challenging.

22 The objective of this paper is to describe a novel method for computing the DRE of
23 ACA. This method attempts to balance the need for computational efficiency with the

1 need for rigorous treatment of aerosol-cloud overlap and small-scale variability of aerosol
2 and clouds. Our method has several unique features: 1) it takes sub-grid scale cloud and
3 aerosol variation into account in DRE computations; 2) it treats the overlap of aerosol and
4 cloud rigorously by utilizing the joint histogram of COD and cloud top pressure (CTP) in
5 the MODIS level-3 product; 3) it is computationally efficient because of the use of a pre-
6 computed look-up table of ACA DRE.

7 In the following sections, we briefly introduce the CALIOP and MODIS data used
8 (Section 2), describe the key assumptions and features of the novel method (Section 3),
9 validate it through comparison with pixel-level computations as in (Meyer et al., 2013)
10 (Section 4), and conclude with a summary and discussion (Section 5).

11 **2. Satellite Data**

12 In (Meyer et al., 2013), the MODIS level-2 cloud product is collocated with CALIOP
13 level-2 aerosol product for every pixel along the CALIOP track and the computation of
14 instantaneous DRE is performed pixel-by-pixel. Then, the pixel-level DRE results are
15 aggregated on a latitude-longitude grid for climatological study. If only the grid-level
16 DRE is of interest, the pixel-by-pixel computation of DRE may not efficient because of
17 redundant computations. For example, if two pixels with the same above-cloud AOD and
18 below-cloud COD occur within the same grid-box, they evidently have the same ACA
19 DRE, but the radiative transfer computation is nevertheless performed twice in the pixel-
20 by-pixel method. As shown in Section 3, a more efficient way is to compute the DRE
21 statistically using the probability density function (PDF) of above-cloud AOD and below-
22 cloud COD. In this study, we use the CALIOP level-2 aerosol and cloud layer product
23 (V3.01) to derive the statistics of ACA properties and the MODIS level-3 daily cloud

1 product for cloud property statistics. It important to note that our method is not limited to
2 CALIOP and MODIS products, but also applicable to other satellite data sets, such as
3 above-cloud aerosol retrievals from POLDER (POLarization and Directionality of
4 the Earth's Reflectances) (Waquet et al., 2009) and OMI (Ozone Monitoring
5 Instrument)(Torres et al., 2012), and cloud retrievals from ISCCP (International Satellite
6 Cloud Climatology Project) (Rossow and Schiffer, 1999) and SEVIRI (Spinning
7 Enhanced Visible and Infrared Imager)(Schulz et al., 2009), as well as outputs from
8 general circulation models and chemical transport models.

9 **2.1. CALIOP level-2 aerosol and cloud layer products**

10 Since its launch in 2006, the space-borne lidar CALIOP has continuously acquired,
11 with near global (albeit instantaneously sparse) coverage, attenuated backscatter
12 measurements at 532 nm and 1064 nm, including linear depolarization information at
13 532nm (Winker et al., 2009). The CALIOP level-2 retrieval algorithm consists of several
14 steps. First, a “feature finder” algorithm and cloud-aerosol discrimination (CAD)
15 algorithm are used to detect aerosol and cloud layers, and record their top and bottom
16 heights and layer integrated properties (Vaughan et al., 2009). Second, the detected
17 aerosol layers are further classified into six sub-types (i.e., polluted continental, biomass
18 burning, desert dust, polluted dust, clean continental and marine) (Omar et al., 2009) and
19 the detected cloud layers are assigned different thermodynamic phases (Hu et al., 2007a)
20 based on the observed backscatter, color ratio and depolarization ratio. Third, *a priori*
21 lidar ratios, pre-selected based on aerosol sub-type and cloud phase, are used to derive the
22 extinction of an aerosol or cloud layer from the attenuated backscatter profile (Young and
23 Vaughan, 2008).

1 In this study, we use CALIOP level-2 version 3.01 aerosol and cloud layer products at
2 a nominal 5 km horizontal resolution (i.e., CAL_LID_L2_05kmALay and
3 CAL_LID_L2_05kmCLay) for aerosol-cloud overlap detection, and for information on
4 aerosol layer properties, including type, aerosol optical depth (AOD), and layer top and
5 bottom height. In addition to physical properties, the CALIOP layer products also provide
6 various metrics and flags on data quality assurance. These include CAD score (Liu et al.,
7 2009), horizontal averaging scale, extinction quality control (QC) flag, and estimated
8 uncertainty of layer AOD. In this study, we apply these metrics following best practices
9 provided by the CALIPSO science team to screen for reliable retrievals (e.g., Winker et
10 al., 2013) (see Table 1).

11 It should be noted here that the current version of CALIOP operational aerosol
12 retrieval algorithm (V3.01) appears to significantly underestimate the AOD of above-
13 cloud aerosol layer according to recent studies (Jethva et al., 2014; Liu et al., 2013;
14 Waquet et al., 2013b). The main reason is that after strong attenuation by the upper part
15 of an aerosol layer, the 532 nm attenuated backscatter of the lower part of aerosol layer is
16 often too small. As a result, it is not included in the current CALIOP retrieval, leading to
17 AOD that is biased low (Jethva et al., 2014; Liu et al., 2013). At the moment, the
18 CALIOP operational team is investigating the possibility of using the algorithm described
19 in (Chand et al., 2008; Hu et al., 2007b) for ACA retrievals (Liu et al., 2013). This
20 alternate method utilizes the reflected lidar signal from the cloud layer underneath to
21 derive the two-way transmittance and thereby the AOD of the ACA layer. Because the
22 backscatter of a cloud layer is usually very strong, the two-way transmittance method is
23 less affected by the strong attenuation of the ACA layer and is therefore expected to

1 alleviate the aforementioned problem. Lidar based AOD retrievals are also known to
2 suffer from other issues, such as the background solar noise during daytime. These issues
3 are beyond the scope of this study, but are nevertheless discussed in the uncertainty
4 analysis of Section 3.4.

5 In addition to retrieval errors and uncertainties, another limitation of CALIOP data is
6 the small sampling rate (i.e., only along track). In order to compute the DRE of ACA
7 over a given latitude-longitude grid box, we assume that the aerosol property statistics
8 retrieved by CALIOP along its narrow track represent the statistics over the whole grid
9 box, i.e., that AOD PDFs are identical. This assumption constitutes an uncertainty in our
10 DRE computation. With no other data available to compare, it is difficult to determine the
11 size of this uncertainty. Recently, several novel methods have been developed to retrieve
12 ACA properties from passive sensor observations (Jethva et al., 2013; Torres et al., 2012;
13 Waquet et al., 2009; 2013a), which will help improve our understanding of the sub-grid
14 ACA variability when they become available to public.

15 Finally, we emphasize two more points. First, none of the aforementioned problems
16 with CALIOP data, e.g., smoke AOD bias, retrieval uncertainties, and small sampling
17 rate, are unique to our method. Any method that uses CALIOP data faces the same
18 challenges. Second, our method is not limited only to CALIOP data. We choose to use
19 CALIOP product in this study solely because it is the only publically available ACA
20 product at the moment. Our method can also be applied to other ACA retrieval products,
21 based on for example, POLDER (Waquet et al., 2009), MODIS (Jethva et al., 2013),
22 OMI (Torres et al., 2012) observations when they become available to public. In fact, as
23 discussed later, the advantage of our method in terms of computational efficiency is even

1 greater when applied on retrievals from passive sensors.

2 **2.2. MODIS daily level-3 cloud property product**

3 This study computes the grid-level ACA DRE using the statistics of aerosol and cloud
4 properties, instead of pixel-by-pixel computation as in (Meyer et al., 2013). We use the
5 Collection 5 (C5) Aqua MODIS level-3 *Daily* gridded Atmosphere product MYD08_D3
6 for the statistics of cloud properties and other parameters, such as solar zenith angle,
7 needed for ACA DRE computations.

8 The MODIS level-3 (i.e., grid-level) product contains statistics computed from a set
9 of level-2 (i.e., pixel-level) MODIS granules. As summarized in (Platnick et al., 2003),
10 the operational level-2 MODIS cloud product provides cloud masking (Ackerman et al.,
11 1998), cloud top height retrieval based on CO₂ slicing or the infrared window method
12 (Menzel et al., 1983), cloud top thermodynamic phase determination (Menzel et al.,
13 2006), and cloud optical and microphysical property retrieval based on the bi-spectral
14 solar reflectance method (Nakajima and King, 1990). In addition to these cloud
15 parameters, the level-2 products also provide pixel-level runtime Quality Assessment
16 (QA) information, which includes product quality as well as processing path information.
17 All MODIS level-2 atmosphere products, including the cloud, aerosol and water vapor
18 products, are aggregated to 1° spatial resolution on a daily (product name MYD08_D3
19 for Aqua MODIS), eight-day (MYD08_E3), and monthly (MYD08_E3) basis.
20 Aggregations include a variety of scalar statistical information (mean, standard deviation,
21 max/min occurrences) and histograms (marginal and joint). A particularly useful level-3
22 cloud product for this study is the daily joint histogram of COD vs. CTP, derived using
23 daily counts of successful daytime level-2 pixel retrievals that fall into each joint COD-

1 CTP bin. Eleven COD bins, ranging from 0 to 100, and 13 CTP bins, ranging from 200 to
2 1000 mb, comprise the histogram. As discussed below, the COD-CTP joint histogram
3 allows for identification of the portion of the cloud population that lies beneath the
4 aerosol layer found by CALIOP, as well as the corresponding COD probability
5 distribution needed for DRE estimation. In addition to the COD-CTP joint histogram, we
6 also use the gridded mean solar and sensor zenith angles for calculating DRE and
7 correcting the COD bias due to the presence of ACA.

8 It should be noted that the level-3 daily product MYD08_D3 contains statistics
9 computed from a set of level-2 MODIS granules that theoretically span a 24-hour interval
10 (Hubanks et al., 2008). However, for cloud parameters retrieved only during daytime,
11 such as COD and cloud droplet effective radius (CER), only daytime level-2 files are
12 used to compute the level-3 daily statistics. These are called *daytime only* SDSs
13 (Scientific Data Sets) in level-3 products. Strictly speaking, the *daytime only* SDSs of
14 only those 1° gridcells between approximately 23° N and 23° S come from a single
15 MODIS overpass. The tropical South East Atlantic region, where transported smoke
16 aerosols are often observed above low-level stratocumulus clouds, is within this range
17 (about 10° N~30° S see Figure 3). The COD statistics in MYD08_D3 product for this
18 region are therefore derived from a single Aqua-MODIS overpass that can be collocated
19 with CALIOP observations (see Section 3.1 for details on collocation). The DRE
20 computed based on the collocated dataset is therefore *instantaneous* DRE at Aqua
21 crossing time (1:30PM) that are directly comparable to the pixel-by-pixel results
22 in (Meyer et al., 2013). Poleward of 23°, MYD08_D3 statistics are derived from
23 averaging several overlapping orbits approximately 100 minutes apart (Hubanks et al.,

1 2008). As a result, strictly speaking for mid and high latitude regions the DRE computed
 2 based on MYD08_D3 data is not *instantaneous* DRE. We emphasize that this is not a
 3 limitation of our method, but an inherent characteristic of the MODIS level-3 product.

4 **3. Methodology**

5 **3.1. Theoretical basis**

6 As in previous investigations (e.g., Chand et al., 2008; 2009; Costantino and Bréon,
 7 2013b; Meyer et al., 2013), we focus on the simplest case of overlapping aerosol and
 8 cloud, i.e., a single layer of aerosol overlying a single layer of low-level liquid-phase
 9 clouds, which is commonly observed in many regions of the globe (Devasthale and
 10 Thomas, 2011). More complex situations certainly exist, such as an aerosol layer located
 11 in between high and low cloud, or an aerosol layer overlying multiple layers of clouds.
 12 However, identification of such situations are either beyond the detection capabilities of
 13 CALIOP or relatively rare (Devasthale and Thomas, 2011). As such, they are not
 14 considered here and left for future research.

15 To illustrate the theoretical foundation of the method, consider the schematic example
 16 in Figure 1. For a given grid box (e.g., $1^\circ \times 1^\circ$ in case of MODIS level-3 data), the gridded
 17 mean *instantaneous* broadband shortwave DRE ($\langle DRE \rangle_{ACA}$) averaged over all ACA
 18 pixels within the grid box is given by:

$$19 \quad \langle DRE \rangle_{ACA} = \int_0^\infty \int_0^\infty DRE(\tau_c, \tau_a) p(\tau_c, \tau_a) d\tau_c d\tau_a, \quad (1)$$

20 where $p(\tau_c, \tau_a)$ is the joint probability density function (PDF) of the above-cloud AOD
 21 at 532 nm (τ_a) and below-aerosol COD (τ_c) of ACA pixels. We note that, in addition to
 22 τ_a , DRE also depends on the the spectral variation of aerosol and cloud optical depth,

1 spectral single scattering albedo and asymmetry factor, wavelength dependencies not
 2 explicitly shown in this equation. These properties are computed using a Mie scattering
 3 code (Wiscombe, 1980) based on the aerosol model described in (Meyer et al., 2013).
 4 The dependencies on solar zenith angle, surface reflectance, cloud particle effective
 5 radius, and atmospheric profile are also omitted from the equation; solar zenith angle and
 6 surface reflectance are expected to have only minor variation within the grid box, while
 7 the impact of cloud particle effective radius and atmospheric profile on shortwave DRE is
 8 relatively small. Since $p(\tau_c, \tau_a)$ describes the covariation of aerosols and clouds for the
 9 ACA pixels, it should ideally be derived from collocated CALIOP aerosol and MODIS
 10 cloud retrievals at pixel level as in (Meyer et al., 2013). This requires large amounts of
 11 pixel-level data, however, as one month of global daytime C5 MODIS level-2 cloud
 12 products in HDF format are roughly 150 Gigabytes. Therefore, pixel-level collocation
 13 and radiative transfer simulation are too computationally expensive and cumbersome for
 14 multiyear global studies.

15 A key assumption in our method, which allows us to avoid tedious pixel-level
 16 collocation, is that the *sub-grid level instantaneous* spatial distribution of above-cloud
 17 AOD is statistically independent from the *sub-grid level instantaneous* spatial distribution
 18 of below-aerosol COD. Under this assumption, $p(\tau_c, \tau_a) = p(\tau_c) \cdot p(\tau_a)$ and Eq. (1)
 19 reduces to:

$$20 \quad \langle DRE \rangle_{ACA} = \int_0^\infty \left[\int_0^\infty DRE(\tau_c, \tau_a) p(\tau_c) d\tau_c \right] p(\tau_a) d\tau_a, \quad (2)$$

21 where $p(\tau_c)$ and $p(\tau_a)$ are the PDF of *instantaneous* below-aerosol COD τ_c and above-
 22 cloud AOD τ_a , respectively, of ACA pixels. The advantage of Eq. (2) is that it allows

1 $p(\tau_c)$ and $p(\tau_a)$ to be derived separately and independently. This assumption is
2 reasonable considering that transported ACAs and low-level boundary layer clouds are
3 usually well separated vertically (Devasthale and Thomas, 2011) and controlled by
4 different meteorological conditions. The potential coupling between the two is that
5 overlying absorbing aerosols could influence the evolution of clouds through changing
6 atmospheric stratification (Wilcox, 2010). However, a recent observational study
7 (Costantino and Bréon, 2013a) found no correlation between above-cloud AOD and
8 below-aerosol COD, although correlations are found between AOD and cloud droplet
9 effect radius, as well as liquid water path. Moreover, it is important to stress that our
10 assumption is that the *instantaneous* above-cloud AOD and below-aerosol COD are
11 independent *at sub-grid scale*. This assumption does not rule out the possibility that AOD
12 and COD could be correlated at longer temporal (e.g., seasonal) and/or larger spatial (e.g.,
13 regional) scale through the thermodynamic and radiative coupling (Wilcox, 2010; 2012).
14 Finally, as shown in section 4, when we compare the DRE derived from pixel-level
15 collocation (i.e., based on Eq. (1)) with that from independent sampling of $p(\tau_c)$ and $p(\tau_a)$
16 (i.e., based on Eq. (2)) the agreement is very good.

17 In our method, the PDF of above-cloud AOD $p(\tau_a)$ is derived from the CALIOP
18 5km aerosol and cloud layer products through the following steps: 1) for each 5km
19 CALIOP profile that falls within a given latitude-longitude grid box, we first search for
20 an aerosol layer; 2) if an aerosol layer is detected and the quality metrics pass the quality
21 assurance criteria summarized in Table 1, we then proceed to check for the presence of an
22 underlying liquid-phase cloud layer within the profile using the CALIOP cloud layer
23 product; 3) if a cloud layer is present, the AOD of the aerosol layer is recorded for the

1 derivation of the $p(\tau_a)$ of the grid box. The bottom height of the aerosol layer is also
2 recorded to derive the grid mean aerosol layer bottom height. Once all of the CALIOP
3 profiles within the grid box are processed, we obtain the PDF of the above-cloud
4 AOD $p(\tau_a)$ and the mean aerosol layer bottom pressure $\langle P_{bottom} \rangle$.

5 As schematically illustrated in Figure 1, the PDF of below-aerosol COD $p(\tau_c)$ is
6 derived from the joint histogram of cloud optical depth and cloud top pressure (COD-
7 CTP joint histogram) in the MODIS daily level-3 product, using the grid mean aerosol
8 layer bottom pressure $\langle p_{bottom} \rangle$ derived above. For a given grid box, we first identify the
9 population of liquid-phase clouds below the pressure level $\langle P_{bottom} \rangle$. This subset, together
10 with the AOD PDF $p(\tau_a)$, is then used to calculate DRE according to Eq. (2).

11 In this study, we focus on the computation of instantaneous DRE. To obtain diurnally
12 averaged DRE, technically speaking one would simply need to integrate over time the
13 instantaneous DRE. However, it is important to note that, in addition to diurnal variation
14 of solar zenith angle, aerosol and cloud properties may also have significant diurnal
15 cycles. In fact, it is known that the low cloud fraction over stratocumulus regimes, such
16 as the South East Atlantic region, have a strong diurnal cycle (15~35% of diurnal mean
17 value) driven by cloud solar absorption (Wood et al., 2002). A recent study by (Min and
18 Zhang, n.d.) indicates that using a constant cloud fraction based on Aqua-MODIS
19 observations tends to result in significantly underestimated diurnal mean DRE even if the
20 diurnal variation of solar zenith angle is considered in the computation. Therefore, the
21 challenge for diurnal DRE computation is to obtain high-temporal-resolution cloud and
22 aerosol observations. In this regard, the SEVIRI on the geostationary satellite MSG

1 (Meteosat Second Generation) may be ideal for a diurnal cycle study since it provides
2 aerosol and cloud observations over the South East Atlantic region at 15 minute intervals.
3 However, a pixel-by-pixel computational approach would be too expensive to be used for
4 the diurnal DRE computation based on high-temporal (15 minutes) and high-spatial (4
5 km at nadir) resolution of SEVERI data. Our method, on the other hand, meets well the
6 demand for computational efficiency.

7 **3.2. DRE Look-up Tables**

8 To speed up calculations, we use pre-computed aerosol-type specific look-up-tables
9 (LUTs), instead of online radiative transfer computation, when deriving the DRE of ACA.
10 The concept of our LUTs is somewhat similar to the “radiative kernels” described in
11 (Hartmann et al., 2001) and (Zelinka et al., 2012) for computing cloud radiative
12 feedbacks. The LUT for each aerosol type consists of DREs at both TOA and surface (not
13 used in this study) for various combinations of AOD, COD, CTP and solar zenith
14 conditions. As such, once the aerosol type and AOD are known from CALIOP and COD,
15 CTP and solar zenith angle are known from MODIS, the corresponding DRE can be
16 obtained through LUT interpolation. Note that the CALIOP only provides AOD at lidar
17 wavelengths (e.g., 532 nm and 1064 nm) for each aerosol type. Therefore, radiative
18 transfer model-appropriate narrowband aerosol scattering properties, namely AOD,
19 single-scattering albedo and asymmetry factor, are needed for the development of the
20 LUT. The current version of LUT focuses on light-absorbing aerosols (e.g., smoke and
21 polluted dust). In order to validate our method with more rigorous pixel-level
22 computations, we adopt the narrowband aerosol optical properties of (Meyer et al., 2013),
23 who used the same radiative transfer code, in the computation of the current LUT. The

1 aerosol model in (Meyer et al., 2013) is extended from an absorbing aerosol model
2 developed for the MODIS Collection 5 Aerosol Product (MOD04) (see Table 4 of Levy
3 et al., 2009). The MOD04 aerosol models define aerosol size distributions and refractive
4 indices based solely on prescribed AOD at 550 nm (MODIS band 4; note that the
5 absorbing aerosol model used here assumes a constant index of refraction, $1.51-0.02i$, at
6 all wavelengths). At AOD=0.5 (550 nm), the single-scattering albedo of this model is
7 about 0.9 over the visible spectral region (see Figure 7 of Meyer et al., 2013), which is in
8 the range of previously reported values (e.g., Keil and Haywood, 2003; Myhre et al.,
9 2003). The current AOD bins (at 550 nm) in the LUT range from 0.05 to 1.5, which
10 covers most of the above-cloud AOD observed by CALIOP. The current COD bins,
11 logarithmically spaced, range from 0.1 to 300. Following the MODIS level-3 data, the
12 thirteen CTP bins range from 1000mb to 200mb. The solar zenith angle bins range from 0
13 to 80 degree. Radiative transfer computations are carried out using the RRTM-SW model
14 (Clough et al., 2005; Iacono et al., 2008). Lambertian ocean surface reflectance is set to
15 5%. Cloud droplet effective radius is fixed at 15 μm , which is close to the global mean
16 value over oceans observed by MODIS (King et al., 2013). This value of effective radius
17 is also used to convert the MODIS visible COD to liquid water path used as input to
18 RRTM-SW. Liquid cloud optical properties are calculated internally by RRTM. For
19 atmospheric profiles of water vapor and temperature, we use NCEP R1 reanalysis data
20 (Kistler et al., 2001) averaged both zonally and annually. Our sensitivity tests indicate
21 that the shortwave **DRE of ACA is largely insensitive to cloud effective radius** or
22 atmospheric profiles.

3.3. Cloud Optical Depth Correction

As noted in previous studies (Coddington et al., 2010; e.g., Haywood et al., 2004), when a cloudy MODIS pixel is contaminated by overlying light-absorbing aerosols the COD retrieval is generally biased low. We have developed a fast COD correction scheme to account for the COD retrieval bias due to ACA in our DRE computation, which is illustrated in Figure 2. This scheme requires both the cloud reflectance LUT for clouds without ACA, for which we use the MODIS operational LUT, and clouds with ACA, for which we use the one developed by Meyer et al. (2013). In the operational MODIS retrieval, the reflectance LUT of cloud without ACA is used to interpret the reflectance of all clouds, including those affected by ACA. Based on this fact, we first infer the “observed” cloud reflectance (after atmospheric correction) by interpolating the reflectance LUT of cloud without ACA corresponding to the biased COD. Then, we use the “observed” cloud reflectance and ACA-affected LUT (derived based on CALIOP AOD) to determine the corrected COD. This COD correction process is performed for every combination of COD bin in $p(\tau_c)$ and AOD bin in $p(\tau_a)$. In the final step we resample the corrected CODs to obtain the corrected $p(\tau_c)$.

It should be noted that because different aerosol type may have different impact on MODIS COD retrievals, the above COD correction process is aerosol-type dependent. In this study, we use light-absorbing aerosols as example to illustrate our method and for validation purposes we use the aerosol model developed by (Meyer et al., 2013) for the development of LUTs for DRE computation and COD correction. However, the LUTs can be easily extended to other aerosol models. In fact, as part of ongoing research, we

1 are extending our LUTs to include all six operational CALIOP aerosol models as
2 described in (Omar et al., 2009).

3 **3.4. Uncertainty Analysis**

4 Several recent studies suggest that the current operational CALIOP product tends to
5 underestimate the above-cloud AOD. Meyer et al. (2013) found that the daytime
6 CALIOP AOD retrievals are systematically smaller than the nighttime retrievals,
7 probably due to the daytime solar background issue. In the light of this finding, Meyer et
8 al. (2013) increased the CALIOP AOD retrievals by a factor of 1.5 to account for the
9 impact of potential AOD bias on DRE of ACA. A more recent case study by (Jethva et
10 al., 2014) suggests that CALIOP ACA AOD retrievals are biased low by a factor of 5 or
11 even more compared with other retrievals, although the generality of this finding needs to
12 be further tested with larger samples. While a rigorous analysis uncertainty analysis of
13 CALIOP AOD product is beyond the scope of this study, it is nevertheless reasonable to
14 assume that the current CALIOP retrievals provide a lower limit to the ACA AOD. In the
15 uncertainty analysis presented in the next section, we carry out two sensitivity tests to
16 estimate the potential impacts of CALIOP AOD bias on DRE computation. We multiply
17 CALIOP AOD values by a factor of 1.5 in the first test following (Meyer et al., 2013) and
18 by a factor of 5 in the second as suggested in (Jethva et al., 2014).

19 Once the magnitude of the uncertainties in the input data is prescribed, the
20 consequential impact on DRE can be easily estimated in our method as follows. First, in
21 addition to the $p(\tau_a)$ based on the original CALIOP data, we also derive the perturbed
22 PDF $\tilde{p}(\tau_a)$ by perturbing the original data according to pre-defined uncertainties (i.e., by

1 increasing the original values by a factor of 1.5 or 5). Then, the impact of input
2 uncertainty on ACA DRE can be estimated by comparing the DREs computed with the
3 original vs. perturbed PDF (i.e., $\langle DRE \rangle_{ACA}$ vs. $\langle \widetilde{DRE} \rangle_{ACA}$). Note that $\langle DRE \rangle_{ACA}$ and
4 $\langle \widetilde{DRE} \rangle_{ACA}$ can be obtained in a single computation because they both represent integrals
5 over $DRE(\tau_c, \tau_a)$, only with different weights. In this regard, our method is much more
6 efficient than the pixel-by-pixel method, in which uncertainty must be estimated by
7 perturbing individual pixels.

8 **4. Implementation and validation of new DRE estimation scheme**

9 Each year during austral winter, dry season biomass burning activities throughout
10 southern Africa inject large amounts of smoke into the troposphere (Eck et al., 2003;
11 Ichoku et al., 2003; Myhre et al., 2003). Prevailing easterly winds during this season
12 often transport the smoke westward off the continent, over the ocean, where extensive
13 marine boundary layer clouds persist for most of the year. Under the descending branch
14 of the Hadley cell, the air mass above the boundary layer is quite dry. Due to the lack of
15 efficient wet scavenging, the transported aerosol layers can remain suspended in the
16 atmosphere for days, creating a near-persistent smoke layer above the stratocumulus deck
17 over the southeastern Atlantic Ocean (Chand et al., 2009; Devasthale and Thomas, 2011;
18 Keil and Haywood, 2003; Wilcox, 2010).

19 To validate our method, we have compared the DRE of above-cloud light-absorbing
20 aerosols in this region with pixel-level computations from (Meyer et al., 2013). Figure 3a
21 shows the seasonal mean (August/September 2007-2011) instantaneous TOA DRE of
22 above-cloud smoke and polluted dust based on the pixel-level computations from (Meyer

1 et al., 2013). Figure 3b shows the corresponding instantaneous TOA aerosol radiative
2 forcing efficiency (RFE) defined as the DRE per unit AOD. The DRE and RFE results
3 computed using our method described in the previous section are shown in Figure 3c and
4 Figure 3d, respectively. Evidently, both DRE and RFE computed using our new method
5 agree closely with the pixel-level computations. Figure 4 shows the meridional mean
6 DRE and RFE for the region using the results in Figure 3. Not surprisingly, the outcomes
7 of the two methods are almost identical. Note that the CODs used in the computations for
8 Figure 3 and Figure 4 are directly from the MODIS products without COD correction.
9 We have also compared the DRE and RFE from the two methods using the corrected
10 COD and achieved again very good agreement (not shown because of close resemblance
11 to Figure 3 and Figure 4). The seasonal and regional mean DRE and RFE, based on the
12 corrected COD, from the pixel-level computation method in (Meyer et al., 2013) are 6.63
13 W m^{-2} and $55.97 \text{ W m}^{-2} \text{ AOD}^{-1}$, respectively (see Table 2). The corresponding values
14 from our new method are 6.39 W m^{-2} and $53.77 \text{ W m}^{-2} \text{ AOD}^{-1}$, respectively.

15 As previously mentioned, to estimate potential bias in CALIOP ACA AOD retrieval
16 on our DRE computation, we carried out two sensitivity tests. We increased CALIOP
17 AOD values by a factor of 1.5 in one test following (Meyer et al., 2013) (hereafter
18 referred to as “x1.5 test”) and by a factor of 5 in another as suggested in (Jethva et al.,
19 2014) (“x5.0 test” hereafter). In both cases, we corrected the MODIS COD retrievals
20 based on the scaled AOD. The regional and seasonal mean DRE of ACA increases, from
21 the original value of 6.39 W m^{-2} to 9.57 W m^{-2} in the x1.5 test and to 30.87 W m^{-2} in the
22 x5.0 test. We have to note that this is a very rough estimate. Nevertheless, the DRE based
23 on the x1.5 scaling of CALIOP AOD seems to agree reasonably with the value, 9.2 ± 6.6

1 W m^{-2} , reported in an independent study by Wilcox (Wilcox, 2012). Interestingly, the
2 scaling of AOD has little impact on RFE in both cases ($53.09 \text{ W m}^{-2} \text{ AOD}^{-1}$ in the x1.5
3 case and $51.24 \text{ W m}^{-2} \text{ AOD}^{-1}$ in the x5.0 case), which apparently suggests a near linear
4 relationship between DRE and AOD as also noted in (Meyer et al., 2013) and (Wilcox,
5 2012) (see his Figure 5).

6

7 In summary, as shown clearly in Figure 3, Figure 4 and Table 2, the DRE inferred
8 from our new method agrees very well with the pixel-level computations. Furthermore,
9 the difference between the two methods is much smaller than, for example, the
10 uncertainty associated with CALIOP retrieval biases.

11 It is worthwhile to clarify again that the results shown in Figure 3 are seasonal mean
12 *instantaneous* DRE at A-Train crossing time (1:30PM local time) based on CALIOP
13 above-cloud AOD and corrected Aqua MODIS below-aerosol COD retrievals. Moreover,
14 the aerosol model described in (Meyer et al., 2013) is used in this study. All these factors
15 should be considered when comparing the results in this study with those in other studies
16 (e.g., Chand et al., 2009; de Graaf et al., 2012; Wilcox, 2012). For example, (Chand et al.,
17 2009) used CALIOP in combination with Terra-MODIS observation to compute the DRE
18 over the South East Atlantic Region. It is known that low-clouds in this region have a
19 strong diurnal cycle driven by solar cloud absorption (Bergman and Salby, 1996;
20 Rozendaal et al., 1995; Wood et al., 2002). As a result the cloud properties observed by
21 Terra-MODIS can be significantly different from those observed by Aqua-MODIS in this
22 region, which could lead to different DRE even if the same method was used.

1 **5. Summary and Discussion**

2 Recent advances in satellite-based remote sensing, in particular the launch of the
3 space-borne lidar CALIOP, have provided an unprecedented opportunity for studying the
4 radiative effects of above-cloud aerosol (ACA). However, the methodologies used in
5 recent studies for computing the ACA DRE appear to be either oversimplified (e.g.,
6 Chand et al., 2009; Oikawa et al., 2013) or too cumbersome (e.g., Meyer et al., 2013).
7 This paper describes a novel method recently developed for computing the shortwave
8 DRE of above-cloud aerosols over ocean. Our method has several unique features
9 compared to previous methods: 1) It takes sub-grid scale cloud and aerosol variation into
10 account in DRE computations, similar to (Meyer et al., 2013); 2) it treats the overlap of
11 aerosol and cloud rigorously by utilizing the joint histogram of COD and CTP in the
12 MODIS level-3 cloud product; 3) it relies on grid-level cloud statistics (i.e., COD-CTP
13 joint histogram), instead of pixel-level products, and utilizes pre-computed look-up tables
14 for ACA DRE computations, making it thus much more efficient than pixel-level
15 computations. As shown in Figure 3, Figure 4 and Table 2, DRE computed using our
16 method agrees well with the pixel-level computations of (Meyer et al., 2013)..

17 In addition to the Southeast Atlantic region, we have recently begun investigating
18 the DRE of above-cloud light-absorbing aerosols for global ocean. Some preliminary
19 results are shown in Figure 5. We first derived the daily grid-level statistics of above-
20 cloud AOD and below-cloud COD, as well as the corresponding ACA DRE, using the
21 method described above and then aggregated the daily means to annual mean. The
22 temporal aggregation is weighted by the number of ACA pixels in each day during 2007-

1 2010. For example, the annual mean ACA DRE in Figure 5c is aggregated from daily
2 mean based on the following equation:

$$3 \quad \overline{\langle DRE \rangle_{ACA}} = \frac{\sum_i N_i \cdot \langle DRE_i \rangle_{ACA}}{\sum_i N_i}, \quad (3)$$

4 where $\langle DRE_i \rangle_{ACA}$ is the mean instantaneous ACA DRE in each day averaged over ACA
5 pixels, N_i is the number of ACA pixels in the grid box in each day, and $\overline{\langle DRE \rangle_{ACA}}$ is the
6 annual mean instantaneous ACA DRE shown in Figure 5c. Figure 5a shows a global map
7 of the annual mean 550 nm AOD of above cloud smoke and polluted dust derived based
8 on 4 years (2007-2010) of CALIOP aerosol and cloud layer products. Similar to
9 (Devasthale and Thomas, 2011), we note several “hotspots” of ACA over the Southeast
10 Atlantic, the East-Central Atlantic off the western coast of Saharan Africa, the Arabian
11 sea, and the North Pacific basin off the coast of eastern Asia. It is interesting to note that
12 the ACA AOD over the east-central Atlantic and Arabian Sea is noticeably larger than
13 that over the southeast Atlantic and North Pacific basin. Figure 5b shows the annual
14 mean below-aerosol COD derived from the MODIS daily level-3 cloud product using the
15 method described in section 3. A notable feature in the figure is that the below-aerosol
16 COD over the North Pacific basin is significantly larger than that over other ACA regions.
17 Figure 5c shows the annual mean shortwave DRE at TOA aggregated from daily values
18 due to ACA smoke and polluted dust over the global ocean. It is intriguing to see that the
19 DRE of ACA over the North Pacific basin is significantly larger than that over the
20 southeast Atlantic, which is in turn larger than the DRE over the east-central Atlantic and
21 the Arabian Sea. In fact, some negative DREs are observed in the latter two regions. This

1 probably due to the COD of below-aerosol clouds being too thin (Figure 5b) over these
2 regions to have significant radiative effect, so that the radiative effect of ACA is close to
3 that of clear skies (i.e., negative). This is interesting because the above-cloud AOD over
4 these regions is actually larger, while the below-aerosol COD over these regions is
5 smaller, compared to their counterparts over the southeast Atlantic and North Pacific
6 basin. Therefore, the preliminary results seem to suggest that the variability of DRE of
7 ACA is modulated by COD, rather than AOD, although it should be noted that we have
8 focused only on the light-absorbing aerosols, i.e., smoke and polluted dust, and assumed
9 the same narrowband scattering properties for them as in (Meyer et al., 2013). Further
10 research is needed to study the impact of aerosol type and scattering properties on the
11 temporal-spatial variation of DRE on global scale. Nevertheless, the preliminary results
12 shown Figure 5 clearly demonstrate the usefulness of our new method for global studies.

13 It should be noted that this study, and previous ones using CALIOP observations
14 (e.g., Chand et al., 2008; Meyer et al., 2013; Oikawa et al., 2013), are limited by the
15 capabilities of CALIOP. Arguably, some aerosols exist above every cloud. However, not
16 all ACA can be detected by CALIOP due to its inherent limitations. Some ACAs are
17 simply too optically thin to be detected, though their radiative effects are also expected to
18 be small. Other situations may also be possible. For example, a confined aerosol layer has
19 larger volume backscatter than a vertically stretched layer, even if the total aerosol
20 amounts are the same, and therefore is more easily detected by CALIOP. Passive sensors,
21 on the other hand, are less affected by the vertical distribution of ACA because they
22 observe column-integrated scattering by aerosols. Recently, several novel techniques
23 have been developed to detect and retrieve ACA properties using passive sensors.

1 (Waquet et al., 2009) developed a method based on multi-angular polarization
 2 measurements from POLDER (Polarization and Directionality of the Earth Reflectances)
 3 to retrieve the AOD of above-cloud smoke. This method has recently been extended to
 4 include both smoke and dust aerosols (Waquet et al., 2013a). Most recently, (Jethva et al.,
 5 2013) demonstrated the ability of a color ratio method to retrieve the above-cloud AOD
 6 based on MODIS multiple spectral cloud reflectance measurements. A review of the
 7 emerging satellite-based observations of above-cloud aerosols can be found in (Yu and
 8 Zhang, 2013). The capabilities and limitations of the passive techniques need to be
 9 systematically studied through inter-comparisons and comparison with CALIOP
 10 observations, but they may provide a complementary perspective on ACA. Recall that
 11 passive imagers have much larger spatial coverage than CALIOP, which makes brute
 12 force calculations of the DRE at the pixel level computationally expensive. In this regard,
 13 our method satisfies the need for efficiency of ACA DRE computations based on passive
 14 imager retrievals.

15 As a final remark, we would like to point out that the ACA DRE discussed in this
 16 study is still a few steps away from the all-sky aerosol radiative effect ($\langle DRE \rangle_{all-sky}$). For
 17 a given grid box, the $\langle DRE \rangle_{all-sky}$ can be decomposed into the sum of clear-sky and
 18 cloudy-sky DRE:

$$19 \quad \langle DRE \rangle_{all-sky} = (1 - f_c) \cdot \langle DRE \rangle_{clear} + f_c \cdot f_{ACA} \cdot \langle DRE \rangle_{ACA}, \quad (4)$$

20 where f_c is the cloud fraction, $\langle DRE \rangle_{clear}$ is the DRE averaged over the clear-sky
 21 portion of the grid box, f_{ACA} is the fraction of cloudy pixels with ACA detected by

1 CALIOP or other sensors, and $\langle DRE \rangle_{ACA}$ is the DRE averaged over all ACA containing
2 pixels. It is important to note an implicit assumption made in Eq. (4), that is, when a
3 distinct ACA layer is not detected, the DRE of ACA is zero. Different sensors (or
4 different retrieval algorithms for the same sensor) may have different sensitivities to
5 ACA and therefore provide different estimates of f_{ACA} and $\langle DRE \rangle_{ACA}$. For example, one
6 sensor may only be able to retrieve ACA for optically thick clouds. This sensor would
7 retrieve a larger $\langle DRE \rangle_{ACA}$, but a smaller f_{ACA} , in comparison with another sensor
8 capable of retrieving ACA for all clouds. Therefore, when comparing the ACA or all-sky
9 DRE estimated based on different instruments or algorithms, it is important to compare
10 both the f_{ACA} and $\langle DRE \rangle_{ACA}$ terms in Eq. (4).

11

1

2 Table 1 Quality control metrics used for screening the CALIOP aerosol layer product.

	Criterion
CAD_score	< -30
Horizontal_averaging	< 20km
Extinction_QC_532	0 or 1
Feature_Optical_Depth_Uncertainty_532	< -99.5

3

4

1

2

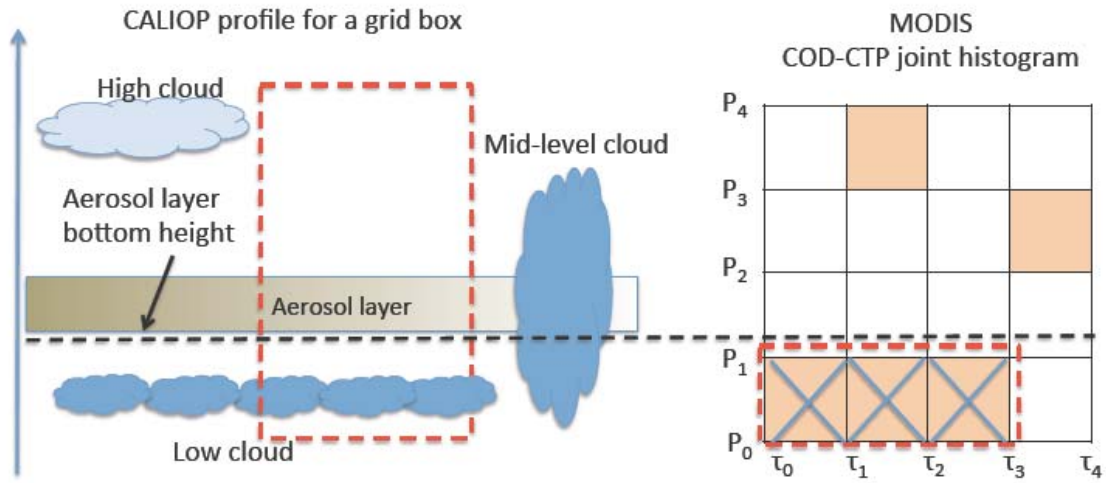
3 Table 2 Regional and seasonal mean values of instantaneous DRE and RFE based on the
4 pixel-level computation and the new method.

	DRE [W m^{-2}]	RFE [$\text{W m}^{-2} \text{AOD}^{-1}$]
	Bias adjusted	Bias adjusted
	(unadjusted)	(unadjusted)
Pixel computation	6.63 (5.92)	55.97 (50.34)
New Method	6.39 (5.77)	53.77 (50.22)

5

6

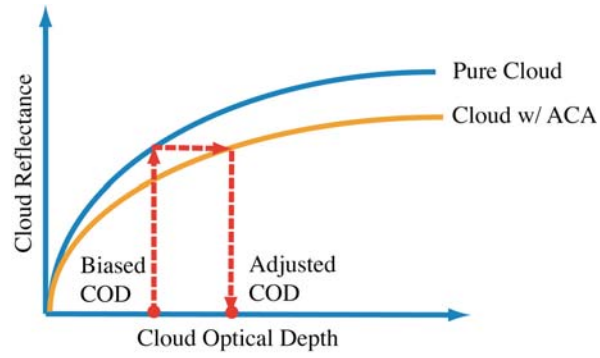
1



2

3 Figure 1 A schematic example to illustrate how CALIOP aerosol layer height information
4 is used in our method to determine the population of liquid-phase clouds below the
5 aerosol layer in the MODIS COD-CTP joint histogram.

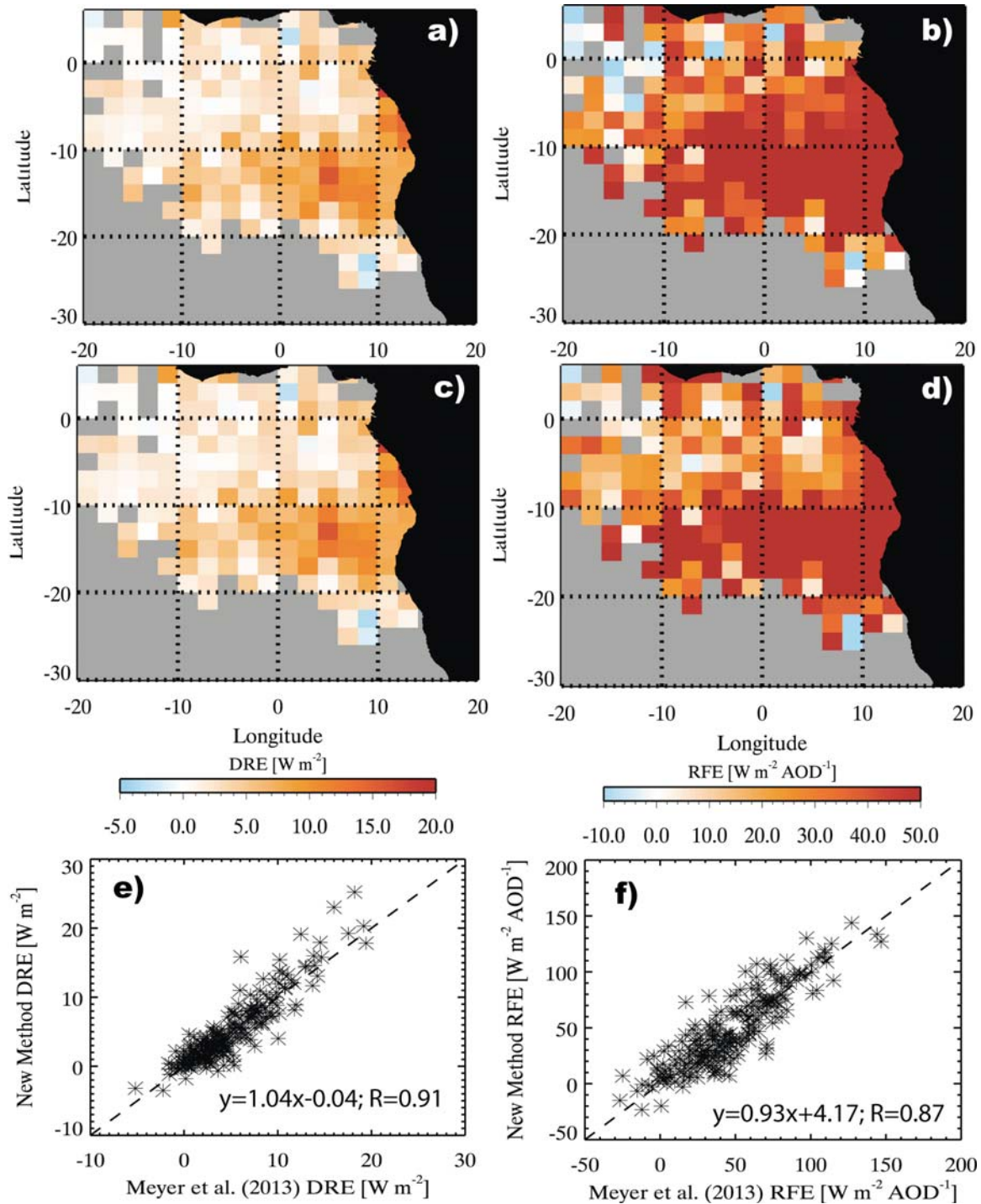
6



1

2 Figure 2 A schematic illustration of our fast scheme to correct the COD retrieval bias in
3 the MODIS cloud product due to overlying aerosol contamination.

4



1

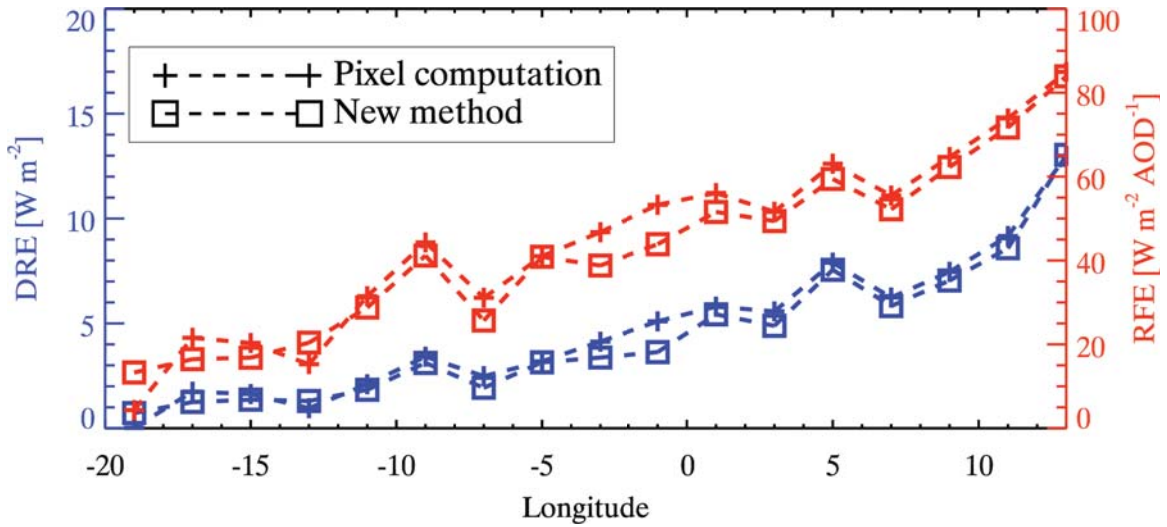
2 Figure 3 a) Seasonal mean (August/September 2007-2011) instantaneous TOA DRE of
 3 above-cloud smoke and polluted dust based on the pixel-level computations from (Meyer
 4 et al., 2013); b) seasonal mean instantaneous TOA aerosol RFE (i.e., DRE per AOD)
 5 from(Meyer et al., 2013); c) same as a), but based on the new method; d) same as b), but
 6 based on the new method.

7

1
2
3
4
5
6

1

2



3

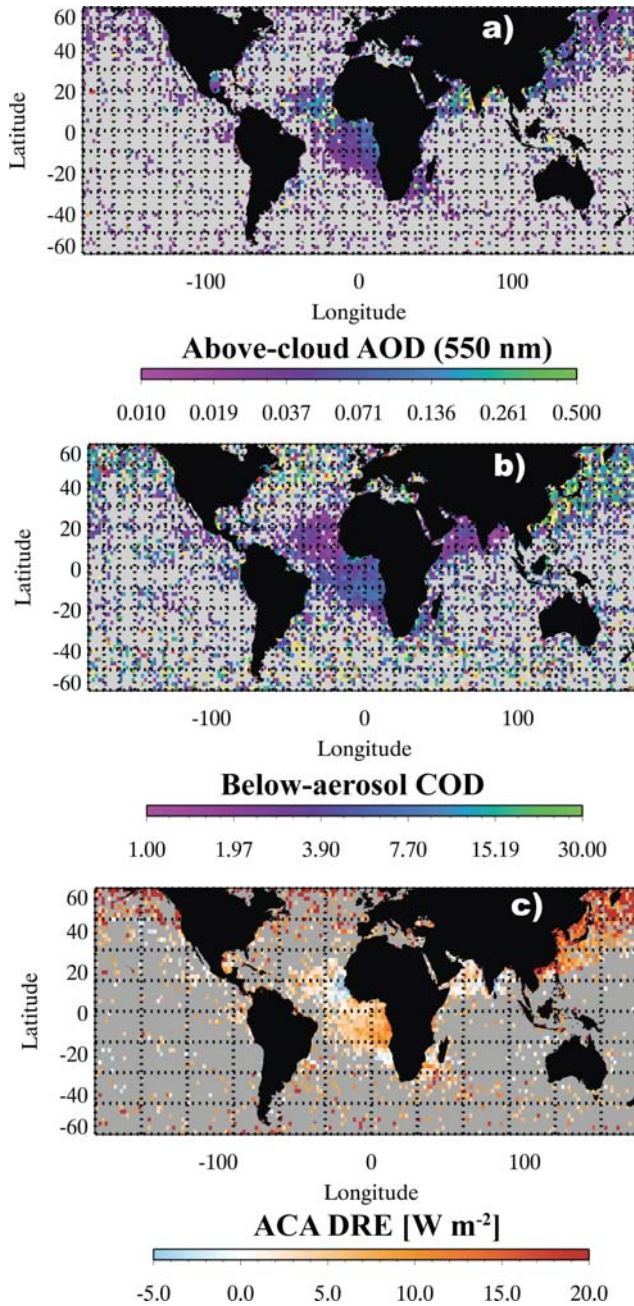
4 Figure 4 Meridional mean DRE and RFE for the region based on the results in Figure 3.

5 Lines with cross symbol correspond to pixel computations from(Meyer et al., 2013).

6 Lines with square symbol correspond to results based on the new method.

7

8



1

2 Figure 5 a) Annual mean AOD (at 550 nm) of above-cloud light-absorbing aerosols (i.e.,
 3 smoke and polluted dust) derived from 4 years (2007~2010) of the CALIOP 5km aerosol
 4 and cloud layer products. b) Annual mean below-aerosol COD derived from the MODIS
 5 daily level-3 COD-CTP joint histogram. c) Annual mean instantaneous TOA DRE of
 6 above-cloud light-absorbing aerosols derived using the new method.

7

1

2 **Reference:**

3 Abel, S. J., Highwood, E. J., Haywood, J. M. and Stringer, M. A.: The direct radiative
4 effect of biomass burning aerosols over southern Africa, *Atmospheric Chemistry and*
5 *Physics*, 5(7), 1999–2018, doi:10.5194/acp-5-1999-2005, 2005.

6 Ackerman, S., Strabala, K., Menzel, W., Frey, R., Moeller, C. and Gumley, L.:
7 Discriminating clear sky from clouds with MODIS, *Journal of Geophysical Research*,
8 103(D24), 32,141–32,157, 1998.

9 Bergman, J. W. and Salby, M. L.: Diurnal Variations of Cloud Cover and Their
10 Relationship to Climatological Conditions, *Journal of Climate*, 9(11), 2802–2820,
11 doi:10.1175/1520-0442(1996)009<2802:DVOCCA>2.0.CO;2, 1996.

12 Chand, D., Anderson, T. L., Wood, R., Charlson, R. J., Hu, Y., Liu, Z. and Vaughan, M.:
13 Quantifying above-cloud aerosol using spaceborne lidar for improved understanding of
14 cloudy-sky direct climate forcing, *J Geophys Res*, 113(D13),
15 doi:10.1029/2007JD009433, 2008.

16 Chand, D., Wood, R., Anderson, T. L., Satheesh, S. K. and Charlson, R. J.: Satellite-
17 derived direct radiative effect of aerosols dependent on cloud cover, *Nature Geoscience*,
18 2(3), 181–184, doi:10.1038/ngeo437, 2009.

19 Clough, S. A., Shephard, M. W., Mlawer, E. J., Delamere, J. S., Iacono, M. J., Cady-
20 Pereira, K., Boukabara, S. and Brown, P. D.: Atmospheric radiative transfer modeling: a
21 summary of the AER codes, *Journal of Quantitative Spectroscopy and Radiative Transfer*
22 VL -, 91(2), 233–244, 2005.

23 Coddington, O. M., Pilewskie, P., Redemann, J., Platnick, S., Russell, P. B., Schmidt, K.
24 S., Gore, W. J., Livingston, J., Wind, G. and Vukicevic, T.: Examining the impact of
25 overlying aerosols on the retrieval of cloud optical properties from passive remote
26 sensing, *J Geophys Res*, 115(D10), doi:10.1029/2009JD012829, 2010.

27 Costantino, L. and Bréon, F. M.: Aerosol indirect effect on warm clouds over South-East
28 Atlantic, from co-located MODIS and CALIPSO observations, *Atmospheric Chemistry*
29 *and Physics*, 13(1), 69–88, doi:10.5194/acp-13-69-2013, 2013a.

30 Costantino, L. and Bréon, F. M.: Satellite-based estimate of aerosol direct radiative effect
31 over the South-East Atlantic, *Atmospheric Chemistry and Physics Discussions*, 13(9),
32 23295–23324, doi:10.5194/acpd-13-23295-2013, 2013b.

33 de Graaf, M., Tilstra, L. G., Wang, P. and Stammes, P.: Retrieval of the aerosol direct
34 radiative effect over clouds from spaceborne spectrometry, *J Geophys Res*, 117(D7),
35 doi:10.1029/2011JD017160, 2012.

36 Devasthale, A. and Thomas, M. A.: A global survey of aerosol-liquid water cloud overlap

1 based on four years of CALIPSO-CALIOP data, *Atmospheric Chemistry and Physics*,
2 11(3), 1143–1154, doi:10.5194/acp-11-1143-2011, 2011.

3 Eck, T. F., Holben, B. N., Ward, D. E., Mukelabai, M. M., Dubovik, O., Smirnov, A.,
4 Schafer, J. S., Hsu, N. C., Piketh, S. J., Queface, A., Roux, J. L., Swap, R. J. and Slutsker,
5 I.: Variability of biomass burning aerosol optical characteristics in southern Africa during
6 the SAFARI 2000 dry season campaign and a comparison of single scattering albedo
7 estimates from radiometric measurements, *J. Geophys. Res.*, 108(D13), 8477,
8 doi:10.1029/2002JD002321, 2003.

9 Hartmann, D., Holton, J. and Fu, Q.: The heat balance of the tropical tropopause, cirrus,
10 and stratospheric dehydration, *Geophys Res Lett*, 28(10), 1969–1972, 2001.

11 Haywood, J. M., Osborne, S. R. and Abel, S. J.: The effect of overlying absorbing aerosol
12 layers on remote sensing retrievals of cloud effective radius and cloud optical depth,
13 *Quarterly Journal of the Royal Meteorological Society*, 130(598), 779–800,
14 doi:10.1256/qj.03.100, 2004.

15 Hu, Y., Vaughan, M., Liu, Z., Lin, B., Yang, P., Flittner, D., Hunt, B., Kuehn, R., Huang,
16 J., Wu, D., Rodier, S., Powell, K., Trepte, C. and Winker, D.: The depolarization -
17 attenuated backscatter relation: CALIPSO lidar measurements vs. theory, *Opt. Express*,
18 15(9), 5327, doi:10.1364/OE.15.005327, 2007a.

19 Hu, Y., Vaughan, M., Liu, Z., Powell, K. and Rodier, S.: Retrieving Optical Depths and
20 Lidar Ratios for Transparent Layers Above Opaque Water Clouds From CALIPSO Lidar
21 Measurements, *Geoscience and Remote Sensing Letters*, IEEE DOI -
22 10.1109/LGRS.2007.901085, 4(4), 523–526, 2007b.

23 Hubanks, P. A., King, M. D., Platnick, S. and Pincus, R.: MODIS atmosphere L3 gridded
24 product algorithm theoretical basis document, *Algorithm Theor. Basis Doc. ATBD-*
25 *MOD*, 30, 2008.

26 Iacono, M. J., Delamere, J. S., Mlawer, E. J., Shephard, M. W., Clough, S. A. and
27 Collins, W. D.: Radiative forcing by long-lived greenhouse gases: Calculations with the
28 AER radiative transfer models, *J. Geophys. Res.*, 113(D13), D13103,
29 doi:10.1029/2008JD009944, 2008.

30 Ichoku, C., Remer, L. A., Kaufman, Y. J., Levy, R., Chu, D. A., Tanré, D. and Holben, B.
31 N.: MODIS observation of aerosols and estimation of aerosol radiative forcing over
32 southern Africa during SAFARI 2000, *J. Geophys. Res.*, 108(D13), 8499,
33 doi:10.1029/2002JD002366, 2003.

34 Jethva, H., Torres, O., Remer, L. A. and Bhartia, P. K.: A color ratio method for
35 simultaneous retrieval of aerosol and cloud optical thickness of above-cloud absorbing
36 aerosols from passive sensors: Application to MODIS measurements, *IEEE*
37 *TRANSACTIONS ON GEOSCIENCE AND REMOTE SENSING*, 51(7), 3862–3870,
38 2013.

- 1 Jethva, H., Torres, O., Waquet, F., Chand, D. and Hu, Y.: How do A-train sensors
2 intercompare in the retrieval of above-cloud aerosol optical depth? A case study-based
3 assessment, *Geophysical Research Letters*, n/a–n/a, doi:10.1002/2013GL058405, 2014.
- 4 Keil, A. and Haywood, J. M.: Solar radiative forcing by biomass burning aerosol particles
5 during SAFARI 2000: A case study based on measured aerosol and cloud properties, *J*
6 *Geophys Res*, 108(D13), 8467, doi:10.1029/2002JD002315, 2003.
- 7 King, M. D., Platnick, S., Menzel, W. P., Ackerman, S. A. and Hubanks, P. A.: Spatial
8 and Temporal Distribution of Clouds Observed by MODIS Onboard the Terra and Aqua
9 Satellites, *IEEE TRANSACTIONS ON GEOSCIENCE AND REMOTE SENSING*,
10 51(7), 3826–3852, doi:10.1109/TGRS.2012.2227333, 2013.
- 11 Kistler, R., Collins, W., Saha, S., White, G., Woollen, J., Kalnay, E., Chelliah, M.,
12 Ebisuzaki, W., Kanamitsu, M., Kousky, V., van den Dool, H., Jenne, R. and Fiorino, M.:
13 The NCEP–NCAR 50–Year Reanalysis: Monthly Means CD–ROM and Documentation,
14 *Bulletin of the American Meteorological Society*, 82(2), 247–267, doi:10.1175/1520-
15 0477(2001)082<0247:TNNYRM>2.3.CO;2, 2001.
- 16 Levy, R. C., Remer, L. A., Tanre, D., Mattoo, S. and Kaufman, Y. J.: Algorithm for
17 remote sensing of tropospheric aerosol over dark targets from MODIS: Collections 005
18 and 051: Revision 2, MODIS Algorithm Theoretical Basis Document for the MOD04_L2
19 Product, 2009.
- 20 Liu, Z., Vaughan, M., Winker, D., Kittaka, C., Getzewich, B., Kuehn, R., Omar, A.,
21 Powell, K., Trepte, C. and Hostetler, C.: The CALIPSOLidar Cloud and Aerosol
22 Discrimination: Version 2 Algorithm and Initial Assessment of Performance, *Journal of*
23 *Atmospheric and Oceanic Technology*, 26(7), 1198–1213,
24 doi:10.1175/2009JTECHA1229.1, 2009.
- 25 Liu, Z., Winker, D. M., Omar, A. H., Vaughan, M., Kar, J., Trepte, C. R. and Hu, Y.:
26 Evaluation of CALIOP 532-nm AOD over Clouds, AGU Fall Meeting 2013, 2013.
- 27 Menzel, P., Frey, R., Baum, B. and Zhang, H.: Cloud Top Properties and Cloud Phase
28 Algorithm Theoretical Basis Document. 2006.
- 29 Menzel, W., Smith, W. and Stewart, T.: Improved Cloud Motion Wind Vector and
30 Altitude Assignment Using VAS, *Journal of Applied Meteorology*, 22(3), 377–384,
31 1983.
- 32 Meyer, K., Platnick, S., Oreopoulos, L. and Lee, D.: Estimating the direct radiative effect
33 of absorbing aerosols overlying marine boundary layer clouds in the southeast Atlantic
34 using MODIS and CALIOP, *Journal of Geophysical Research–Atmospheres*, n/a–n/a,
35 doi:10.1002/jgrd.50449, 2013.
- 36 Min, M. and Zhang, Z.: **On the influence of cloud fraction diurnal cycle and sub-grid
37 cloud optical thickness variability on all-sky direct aerosol radiative forcing**

1 , Journal of Quantitative Spectroscopy and Radiative Transfer, ((submitted)), n.d.

2 Myhre, G., Berntsen, T. K., Haywood, J. M., Sundet, J. K., Holben, B. N., Johnsrud, M.
3 and Stordal, F.: Modeling the solar radiative impact of aerosols from biomass burning
4 during the Southern African Regional Science Initiative (SAFARI-2000) experiment, J.
5 Geophys. Res., 108(D13), 8501, doi:10.1029/2002JD002313, 2003.

6 Nakajima, T. and King, M.: Determination of the optical thickness and effective particle
7 radius of clouds ..., J Atmosph Sci, 1990.

8 Oikawa, E., Nakajima, T., Inoue, T. and Winker, D.: A study of the shortwave direct
9 aerosol forcing using ESSP/CALIPSO observation and GCM simulation, J Geophys Res,
10 118, 3687–3708, doi:10.1002/jgrd.50227, 2013.

11 Omar, A. H., Winker, D. M., Vaughan, M. A., Hu, Y., Trepte, C. R., Ferrare, R. A., Lee,
12 K.-P., Hostetler, C. A., Kittaka, C. and Rogers, R. R.: The CALIPSO automated aerosol
13 classification and lidar ratio selection algorithm, Journal of Atmospheric and Oceanic
14 Technology, 26(10), 1994–2014, 2009.

15 Oreopoulos, L., Cahalan, R. F. and Platnick, S.: The Plane-Parallel Albedo Bias of Liquid
16 Clouds from MODIS Observations, Journal of Climate, 20(20), 5114–5125,
17 doi:10.1175/JCLI4305.1, 2007.

18 Platnick, S., King, M., Ackerman, S., Menzel, W., Baum, B., Riedi, J. and Frey, R.: The
19 MODIS cloud products: algorithms and examples from Terra, Geoscience and Remote
20 Sensing, IEEE Transactions on, 41(2), 459–473, 2003.

21 Rossow, W. B. and Schiffer, R. A.: Advances in Understanding Clouds from ISCCP,
22 Bulletin of the American Meteorological Society, 80(11), 2261–2287, doi:10.1175/1520-
23 0477(1999)080<2261:AIUCFI>2.0.CO;2, 1999.

24 Rozendaal, M. A., Leovy, C. B. and Klein, S. A.: An Observational Study of Diurnal
25 Variations of Marine Stratiform Cloud, Journal of Climate, 8, 1795–1809, 1995.

26 Schulz, J., Albert, P., Behr, H. D., Caprion, D., Deneke, H., Dewitte, S., Dürr, B., Fuchs,
27 P., Gratzki, A., Hechler, P., Hollmann, R., Johnston, S., Karlsson, K. G., Manninen, T.,
28 Müller, R., Reuter, M., Riihelä, A., Roebeling, R., Selbach, N., Tetzlaff, A., Thomas, W.,
29 Werscheck, M., Wolters, E. and Zelenka, A.: Operational climate monitoring from space:
30 the EUMETSAT Satellite Application Facility on Climate Monitoring (CM-SAF),
31 Atmospheric Chemistry and Physics, 9(5), 1687–1709, doi:10.5194/acp-9-1687-2009,
32 2009.

33 Schulz, M., Textor, C., Kinne, S., Balkanski, Y., Bauer, S., Berntsen, T., Berglen, T.,
34 Boucher, O., Dentener, F., Guibert, S., Isaksen, I. S. A., Iversen, T., Koch, D., Kirkevåg,
35 A., Liu, X., Montanaro, V., Myhre, G., Penner, J. E., Pitari, G., Reddy, S., Seland, Ø.,
36 Stier, P. and Takemura, T.: Radiative forcing by aerosols as derived from the AeroCom
37 present-day and pre-industrial simulations, Atmos. Chem. Phys, 6, 5225–5246, 2006.

1 Stier, P., Schutgens, N. A. J., Bellouin, N., Bian, H., Boucher, O., Chin, M., Ghan, S.,
2 Huneus, N., Kinne, S., Lin, G., Ma, X., Myhre, G., Penner, J. E., Randles, C. A.,
3 Samset, B., Schulz, M., Takemura, T., Yu, F., Yu, H. and Zhou, C.: Host model
4 uncertainties in aerosol radiative forcing estimates: results from the AeroCom Prescribed
5 intercomparison study, *Atmospheric Chemistry and Physics*, 13(6), 3245–3270,
6 doi:10.5194/acp-13-3245-2013, 2013.

7 Torres, O., Jethva, H. and Bhartia, P. K.: Retrieval of Aerosol Optical Depth above
8 Clouds from OMI Observations: Sensitivity Analysis and Case Studies,
9 <http://dx.doi.org/10.1175/JAS-D-11-0130.1>, 69(3), 1037–1053, doi:10.1175/JAS-D-11-
10 0130.1, 2012.

11 Twomey, S.: *Atmospheric aerosols*, Elsevier Scientific Publishing Co., New York, NY.
12 1977.

13 Vaughan, M. A., Powell, K. A., Winker, D. M., Hostetler, C. A., Kuehn, R. E., Hunt, W.
14 H., Getzewich, B. J., Young, S. A., Liu, Z. and McGill, M. J.: Fully Automated Detection
15 of Cloud and Aerosol Layers in the CALIPSO Lidar Measurements, *J. Atmos. Oceanic*
16 *Technol.*, 26(10), 2034–2050, doi:doi: 10.1175/2009JTECHA1228.1, 2009.

17 Waquet, F., Cornet, C., Deuzé, J. L., Dubovik, O., Ducos, F., Goloub, P., Herman, M.,
18 Lapyonok, T., Labonnote, L. C., Riedi, J., Tanre, D., Thieuleux, F. and Vanbauce, C.:
19 Retrieval of aerosol microphysical and optical properties above liquid clouds from
20 POLDER/PARASOL polarization measurements, *Atmos. Meas. Tech.*, 6(4), 991–1016,
21 doi:10.5194/amt-6-991-2013, 2013a.

22 Waquet, F., Peers, F., Ducos, F., Goloub, P., Platnick, S., Riedi, J., Tanré, D. and
23 Thieuleux, F.: Global analysis of aerosol properties above clouds, *Geophysical Research*
24 *Letters*, n/a–n/a, doi:10.1002/2013GL057482, 2013b.

25 Waquet, F., Riedi, J., Labonnote, L. C., Goloub, P., Cairns, B., Deuzé, J. L. and Tanre,
26 D.: Aerosol Remote Sensing over Clouds Using A-Train Observations, *J Atmosph Sci*,
27 66(8), 2468–2480, doi:10.1175/2009JAS3026.1, 2009.

28 Wilcox, E. M.: Stratocumulus cloud thickening beneath layers of absorbing smoke
29 aerosol, *Atmospheric Chemistry and Physics*, 10(23), 11769–11777, doi:10.5194/acp-10-
30 11769-2010, 2010.

31 Wilcox, E. M.: Direct and semi-direct radiative forcing of smoke aerosols over clouds,
32 *Atmospheric Chemistry and Physics*, 12(1), 139–149, doi:10.5194/acp-12-139-2012,
33 2012.

34 Winker, D. M., Tackett, J. L., Getzewich, B. J., Liu, Z., Vaughan, M. A. and Rogers, R.
35 R.: The global 3-D distribution of tropospheric aerosols as characterized by CALIOP,
36 *Atmospheric Chemistry and Physics*, 13(6), 3345–3361, doi:10.5194/acp-13-3345-2013,
37 2013.

38 Winker, D. M., Vaughan, M. A., Omar, A., Hu, Y., Powell, K. A., Liu, Z., Hunt, W. H.

- 1 and Young, S. A.: Overview of the CALIPSO mission and CALIOP data processing
2 algorithms, *Journal of Atmospheric and Oceanic Technology*, 26(11), 2310–2323, 2009.
- 3 Wiscombe, W. J.: Improved Mie scattering algorithms, *Applied Optics*, 19(9), 1505–
4 1509, 1980.
- 5 Wood, R., Bretherton, C. S. and Hartmann, D. L.: Diurnal cycle of liquid water path over
6 the subtropical and tropical oceans, *Geophysical Research Letters*, 29(23), 2092–,
7 doi:10.1029/2002GL015371, 2002.
- 8 Young, S. A. and Vaughan, M. A.: The Retrieval of Profiles of Particulate Extinction
9 from Cloud-Aerosol Lidar Infrared Pathfinder Satellite Observations (CALIPSO) Data:
10 Algorithm Description, *J. Atmos. Oceanic Technol.*, 26(6), 1105–1119, doi:doi:
11 10.1175/2008JTECHA1221.1, 2008.
- 12 Yu, H. and Zhang, Z.: New Directions: Emerging satellite observations of above-cloud
13 aerosols and direct radiative forcing, *Atmospheric Environment*, 72(0), 36–40,
14 doi:10.1016/j.atmosenv.2013.02.017, 2013.
- 15 Yu, H., Kaufman, Y. J., Chin, M., Feingold, G., Remer, L. A., Anderson, T. L.,
16 Balkanski, Y., Bellouin, N., Boucher, O. and Christopher, S.: A review of measurement-
17 based assessments of the aerosol direct radiative effect and forcing, *Atmospheric*
18 *Chemistry and Physics*, 6(3), 613–666, 2006.
- 19 Zelinka, M. D., Klein, S. A. and Hartmann, D. L.: Computing and partitioning cloud
20 feedbacks using cloud property histograms. Part I: Cloud radiative kernels, *Journal of*
21 *Climate*, 25(11), 3715–3735, doi:10.1175/JCLI-D-11-00248.1, 2012.

22